Title:
An Efficient Algorithm for Detecting Flatness of Small Metal Parts Based on Stereo Matching of Multi-Similarity Fusion

Authors:
Liangang Xie, liangangxie@sjtu.edu.cn, Shanghai Jiao Tong University
Xianda Li, sbnine@sjtu.edu.cn, Shanghai Jiao Tong University
Xiangzhi Wei, antonwei@sjtu.edu.cn, Shanghai Jiao Tong University

Keywords:
Boundary Detection, Flatness Measurement, Stereo Matching, Metal Parts

DOI: 10.14733/cadconfP.2020.131-136

Introduction:
Metal covers for the PCB chips are required to be flat upon a maximum error of 0.1mm such that they can be pasted to flat zones of the PCB stably. These metal covers are widely used, which require a fast flatness detection to save production time and cost. Binocular stereo vision is an effective means of detecting the boundaries of the metal parts. However, the precise boundaries of the metal parts are not straightforward to be identified due to the reflection, angle of the cameras in taking the images, and the parameters of the cameras. To speed up the detection process while reducing the measurement errors, we proposed a hybrid strategy by combining Canny operator, Zernike moment operator and linear interpolation to achieve subpixel-level precision efficiently. According to the triangulation principle [1], as long as the matching relations of the same boundary points on left and right images are obtained, their corresponding 3D coordinates can be reconstructed. To solve the ambiguity problem while sparse stereo matching of boundary points, a stereo matching algorithm based on a similarity fusion of shape, gradient and disparity is proposed. The methodology is tested on a set of metal covers and is compared with the laser profiler and the structured light method to validate its effectiveness. The experimental results show that our proposed method has high precision and efficiency for small metal covers.

Main Idea:
Hybrid Subpixel-Boundary Detection Algorithm

For tiny metal parts like metal covers, there are mainly two types of warpage under normal stress including bending and twisting. When two types of warpage occur, the points with the largest amount of warping all belong to the boundary points of the parts. So the warping degree (or flatness) of the metal parts can be measured by calculating the maximum height differences between all boundary points and the plane.

In order to reconstruct the 3D coordinates of all boundary points, the 2D boundary detection should be conducted on the image to get 2D coordinates of the boundary. The precision of 2D boundary detection directly affects the accuracy of the resultant 3D coordinates. Boundary detection algorithms focus on pixel-level and subpixel-level precisions [2]. The subpixel boundary detection algorithms can overcome the limits of the physical resolution of CCD cameras and achieve an extremely high accuracy [3]. However, if a subpixel detection algorithm is applied to each pixel, it will be extremely time-consuming and not suitable for industrial applications with real-time requirements [4]. In order to balance the efficiency and accuracy, we propose a hybrid algorithm of Canny, Zernike and linear interpolation and take their respective advantages. Refer to Fig. 1, the Canny operator is first used to detect the green integer pixel point; then the Zernike operator [5] is applied to detect the blue subpixel

© 2020 CAD Solutions, LLC, http://www.cad-conference.net

points. Since common stereo matching algorithms match the points on the same row from the left and right images [1], a linear interpolation can be applied to obtain resulting subpixel points (orange) based on the horizontal lines of the pixel map and the boundary curve (blue) derived by the Zernike operator. Due to the limited space, the specific formulas for this part are not derived in detail here.

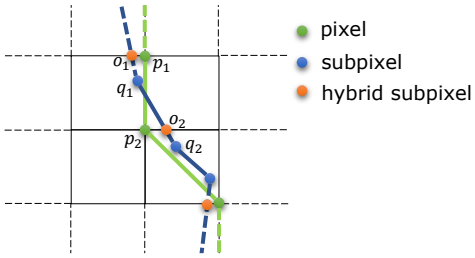

Fig. 1: Schematic diagram of hybrid subpixel-boundary detection algorithm.

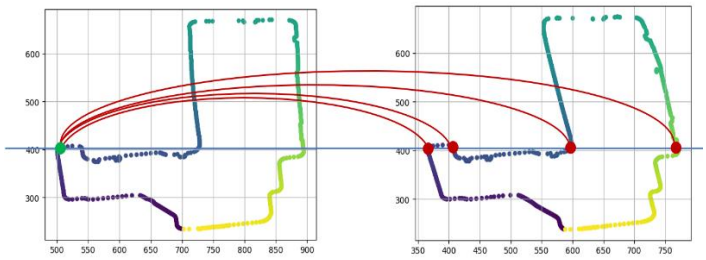

Fig. 2: One point on the left image may be mismatched to a set of points on the right image.

Similarity Fusion of Shape, Gradient and Disparity

Matching the corresponding points of left and right images accurately and efficiently is a challenge in 3D measurement. For example, in Fig. 2, the red dots on the right image are candidate points that may match the same green dot on the left image. Therefore, a robust similarity measurement is required to evaluate the similarity of each pair of matching points. Unlike traditional dense stereo matching, in our task the boundary points to be matched are sparse, discrete, and non-integral, which increase the difficulties of precise matching since their shape and texture features are highly similar. To address this issue, we propose a similarity fusion of shape, gradient and disparity to calculate the matching information at each pair of points.

For ease of computation, for each boundary point, we create a window centered at this point with its nearest neighboring integer pixels included in the window. The size of the window is $N \times N$, where N can be adjusted to increase/reduce the number of neighboring pixels used for computation.

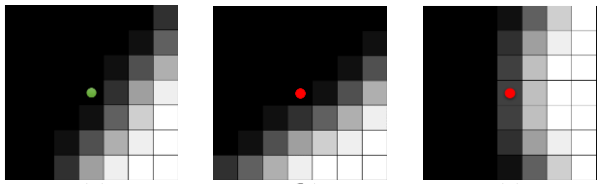

(a) (b) (c)

Fig. 3: (a) A window at a point on the left image, (b) and (c): Windows at two different points on the right image.

In Fig. 3, Fig. 3(a) is a window of a point (green) in the left image. Fig. 3(b) and (c) are the windows of two points (red) of the right image. It can be seen intuitively that (b) is more similar to (a) than (c). In order to describe this kind of similarity, as shown in Eqn. (1.1), the square sum of the difference of the gray values in the corresponding positions of two windows is used.

$$C_{SSD}(p,d) = \sum_{s=1}^{N}\sum_{t=1}^{N}\left[I_R(s,t) - I_L(s,t)\right]^2 \tag{1.1}$$

where I_L is the gray value of left pixel p and I_R is the gray value of right pixel q. And d is the difference of the x-coordinates of the current pair of points to be matched, which is usually called

© 2020 CAD Solutions, LLC, http://www.cad-conference.net

disparity. When the difference between the gray values of two windows is small, $C_{SSD}(p,d)$ is also small. Note that $C_{SSD}(p,d)$ is sensitive to the shape difference of the distribution of the neighborhood of a point at the center of the left image and that of another point at the center of the right image, so we call it *shape similarity measurement*.

Although $C_{SSD}(p,d)$ can describe the similarity of shapes, it is sensitive to random noise. To mitigate this, we further exploit the gradient information of the points. Based on the results of Zernike operator, a similarity measurement for boundary gradients is proposed in Eqn. (1.2). This equation combines the amplitude component and angle component of the gradient calculated by integral, and thus is very robust to noise and illumination changes.

$$C_{dir}(p,d) = (\left\|\vec{p}\right\| - \left\|\vec{q}\right\|) / (k * (\left\|\vec{p}\right\| + \left\|\vec{q}\right\|) * (\cos\left\langle \vec{p},\vec{q} \right\rangle + \sigma)) \tag{1.2}$$

where $\left\|\vec{p}\right\|$ and $\left\|\vec{q}\right\|$ denote the average gradient amplitudes of all subpixel boundary points in the window of left pixel p and right pixel q respectively, and they can be expressed as the average gray step value h_L and h_R of all points in the window centered on p and q respectively; angle $\left\langle \vec{p},\vec{q} \right\rangle$ is the difference of the angle of the average gradient direction of all points in the window; k is a coefficient used to measure the relative importance of the gradient amplitude to the angle, and $k > 0$; σ is a correction factor that ensures the denominator is non-zero.

$$C_{dir}(p,d) = \left(\left| \frac{1}{n_L} \sum_{i=1}^{n_L} h_{Li} - \frac{1}{n_R} \sum_{i=1}^{n_R} h_{Ri} \right| \right) / \left(k * \left| \frac{1}{n_L} \sum_{i=1}^{n_L} h_{Li} + \frac{1}{n_R} \sum_{i=1}^{n_R} h_{Ri} \right| * \left(\cos\left\langle \frac{1}{n_L} \sum_{i=1}^{n_L} \overrightarrow{h_{Li}}, \frac{1}{n_R} \sum_{i=1}^{n_R} \overrightarrow{h_{Ri}} \right\rangle + \sigma \right) \right) \tag{1.3}$$

In order to evaluate the reliability of the disparity of the current pair of points, a reference disparity d_{ref} is introduced. The disparity values solved in the window are close to the disparity of the central point in the window, and their average can be used as reference disparity d_{ref} to evaluate the credibility of the disparity of the central point. Based on d_{ref}, the disparity similarity measurement can be obtained by Eqn. (1.4).

$$C_{dis} = \frac{x_L - x_R - d_{ref}}{\beta_0 + n * \Delta\beta}, \text{ where } d_{ref} = \begin{cases} \dfrac{\sum_{i=1}^{n} d_i}{n} & if\ \exists\ subpixels\ p_1, p_2, \ldots, p_n \in N(p) \\ \lambda(x_L - x_R) & ,else \end{cases} \tag{1.4}$$

where $N(p)$ represents a window centered at p and n represents the number of boundary points in $N(p)$; x_L and x_R represent the x-coordinates of the left and right pixels to be matched respectively; λ is a scale factor, which determines the relative value of the reference disparity d_{ref} when no matched pixels exist in the window. $\beta_0 + n * \Delta\beta$ represents the credibility of the reference disparity: The more matched points in the window, the higher the credibility of the reference disparity d_{ref}.

To comprehensively consider the shape, gradient and disparity features of the boundary pixels, the above three similarity measurements are weighted and summed up to obtain a multi-similarity measurement fusion as Eqn. (1.5) shows.

$$S(p,d) = \alpha C_{SSD} + \beta C_{dir} + \gamma C_{dis} \tag{1.5}$$

where α, β and γ are the coefficients that control the relative importance of three similarity measurements. The multiple possible values of each coefficient are combined according to the orthogonal table, and the optimal parameter combination is obtained by comparing and analyzing the

© 2020 CAD Solutions, LLC, http://www.cad-conference.net

corresponding experimental results of each combination. For a pixel in the left image, the multi-similarity measurement is calculated for each pixel on the same line in the right image. The "Winner Take All" strategy (WTA) is adopted: the pixel with the smallest multi-similarity measurement is selected as the corresponding matching pixel and the disparity of pixel p can be obtained as $d = \arg\min_d S(p,d)$.

Experiments:

Measurement Accuracy and Efficiency Experiment

The binocular vision system used for our experiment is shown in Fig. 4(a) and the 3D point cloud of the boundary of the metal part reconstructed by our method is shown in Fig. 4(b).

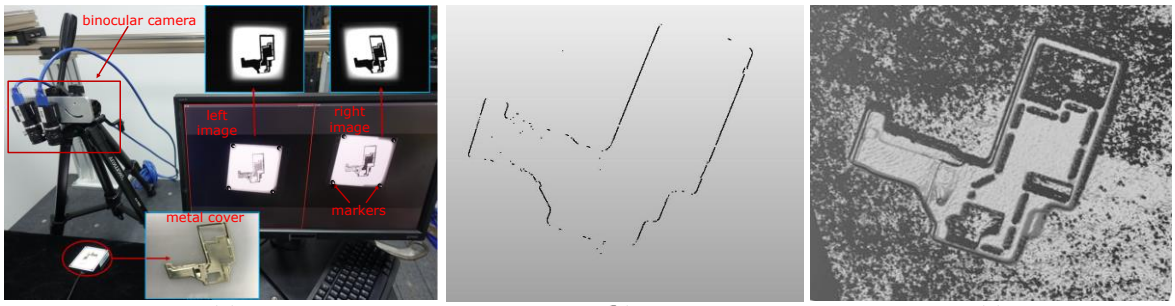

(a) (b) (c)

Fig. 4: (a) The binocular vision system using our proposed 3D boundary reconstruction algorithm; (b) the sparse 3D point cloud of the part's boundary reconstructed by our method; (c) the dense point cloud of the part's surface reconstructed by the structured light equipment.

As a conventional non-contact measurement method, the laser profiler owns a measuring precision of 0.001mm, though it needs a set of expensive auxiliary mechanisms such as high-precision sliding guides and servo motors. Therefore, we applied the laser profiler to the measurement of the metal cover for 100 times and took the average value as the truth value. To evaluate the accuracy and efficiency of the proposed method, we measured the largest distance from all points of one part to the plane by the laser profiler, the structured light system and our method. The results of average μ, variance σ^2 and relative error of each method were obtained by 100 times of repeative measurements. Meanwhile, to evaluate the speed and economics of each method, we listed the time consuming per measurement and cost of the hardwares required in each method. The hardwares in three scheme are the models commonly used and have certain representativeness. The results obtained are shown as Tab. 1.

Methods	$\mu(mm)$	$\sigma^2(mm^2)$	$error(\%)$	$time(ms)$	*hardware cost*($)
Laser profiler	0.323	8.5e-4	N/A	1280	~8000
Structured light system	0.352	5.6e-3	8.978	1590	~1700
Our method	0.337	3.2e-3	4.334	627	~800

Tab. 1: The accuracy, error, speed and cost of three schemes.

Note: In Tab. 1, 'N/A' means that the measurement results of the laser profiler are used as the truth value.

The results of the experiment show that the laser profiler owns the highest measurement precision and smallest variance. However, its hardware cost is significantly higher than other two methods, about 5000~10000 dollars for each laser profiler.

The structured light system has a relatively high variance and error in the measurement of small metal parts. It needs to project multiple stripes in the reconstruction process, which could introduce

© 2020 CAD Solutions, LLC, http://www.cad-conference.net

noise by reflecting light on the boundary as shown in Fig. 4(c). For smooth and shining object, some special powder is often used to cover on reflective areas to mitigate the reflection problem. But this process is obviously not suitable for the rapid measurement of small metal parts.

The precision of our method is between the precision of the laser profiler and the structured light system. And the proposed method has an obvious advantage in the measurement efficiency due to the fact that the proposed method only needs one shot of left and right cameras and that only the boundary of the part is reconstructed, without using additional operations like projecting multiple stripes or reconstructing the whole surface. Moreover, the proposed method has an obvious cost advantage and can be regarded as a low-cost alternative scheme for industrial applications.

Measurement Stability Experiment

In order to evaluate the stability of our method, we further tested 200 small metal parts using our method, and compare the measurement results with the results of the laser profiler and structured light system. According to the flatness, 200 small metal parts are divided into qualified and unqualified categories. We denote by true positive (TP), false positive (FP), true negative (TN) and false negative (FN) as the numbers of the defective unqualified, the defective qualified, the defect-free qualified and the defect-free unqualified parts, respectively. Let P_r be the ratio of correctly detected unqualified parts w.r.t the total detected unqualified parts; let R_c be the ratio of correctly detected unqualified parts w.r.t the total real unqualified parts; and let A_{cc} be the ratio of correct inspection results. They can be expressed as follows:

$$P_r = \frac{TP}{TP+FP},\ R_c = \frac{TP}{TP+FN},\ A_{cc} = \frac{TP+TN}{TP+TN+FP+FN} \tag{1.6}$$

The flatness detection results for the metal parts are shown in Tab. 2.

Methods	P_r(%)	R_c(%)	A_{cc}(%)
Laser profiler	100	100	100
Structured light system	96.25	97.47	97.50
Our method	97.50	98.74	98.50

Tab. 2: The flatness detection results for batch metal parts.

In Tab. 2, the results for the laser profile are all 100% because we take the results of the laser profiler as the truth values. Compared with the truth values, the vast majority of unqualified parts can be correctly detected and classified by the other two methods. However, according to the flatness detection results, our proposed method is more accurate and stable than the structured light system.

Although the proposed method has excellent performance and cost advantage in detecting the flatness of small metal parts, it is not universal and has some limitations. Because the flatness is measured by reconstructing the bottom boundaries in the proposed method. When the thickness of parts exceeds a threshold (e.g., 3mm), it will induce occlusion or shadow at the boundaries, which will cause non-negligible measurement errors. Finally, limited by the field of view of the cameras, the proposed method is not suitable for the measurement of large parts.

References:

[1] Richard, H.; Andrew, Z.: Multiple View Geometry in Computer Vision, Cambridge University Press, Canberra, 2004.

[2] Marr, D.; Hildreth, E.: Theory of edge detection, Proceedings of the Royal Society of London, 207(1167), 1980, 187-217. https://doi.org/10.1098/rspb.1980.0020

[3] Papari, G.; Petkov, N.: Edge and line-oriented contour detection: State of the art, Image and Vision Computing, 29(2-3), 2011, 79-103. http://doi.org/10.1016/j.imavis.2010.08.009

© 2020 CAD Solutions, LLC, http://www.cad-conference.net

[4] Cui, Y.; Schuon, S.; Thrun, S.: Algorithms for 3D shape scanning with a depth camera, IEEE Transactions on Pattern Analysis and Machine Intelligence, 35(5), 2013, 1039-1050. http://doi.org/10.1109/TPAMI.2012.190

[5] Ghosal, S.; Mehrotra, R.: Orthogonal moment operators for sub-pixel edge detection, Pattern Recognition, 26(10), 1993, 295-306.

© 2020 CAD Solutions, LLC, http://www.cad-conference.net